

Electron identification and b-tagging with the road method

F. Beaudette and J.-F. Grivaz

Laboratoire de l'Accélérateur Linéaire – Orsay

D0 note 4032

October 3, 2002

Abstract

The road method, an algorithm for the identification of electrons in jets, has been applied to data collected during the first semester of 2002. The efficiency and the purity have been evaluated using J/ψ and K_S^0 signals. Evidence for b-jet tagging with electrons has been obtained.

1 Introduction

The road method, an algorithm for the identification of electrons in jets, has been extensively described in Ref. [1]. In the present study, its performance on real data is assessed. The data sample was collected during the first semester of 2002. The electron identification efficiency and the mistagging rate have been determined using signals of $J/\psi \rightarrow e^+e^-$ and $K_S^0 \rightarrow \pi^+\pi^-$, respectively. The b-tagging performance has been investigated using a sample of events containing a high p_T muon, therefore enriched in b-jets.

2 Datasets

The data sample used consists of approximately 48 million events recorded from February to May 2002. They were reconstructed with versions p10.15.00, p10.15.01 and p10.15.02 of DORECO. The differences between those versions are irrelevant for the present study.

The Monte Carlo samples consist of

- 9074 direct J/ψ 's produced with $p_T > 10 \text{ GeV}/c$ and $|\eta| < 1.5$.
- 1000 QCD $b\bar{b}$ events, produced with a \hat{p}_T in the hard process greater than $20 \text{ GeV}/c$.
- A Monte Carlo sample of generic QCD events, also produced with $\hat{p}_T > 20 \text{ GeV}/c$. The events with at least one track with $p_T > 1.5 \text{ GeV}/c$ matched to a pion coming from a K_S^0 decay have been selected. The sample thus obtained contains 929 events.

All these Monte Carlo samples were generated with PYTHIA, simulated with mcp10 with plate geometry, and reconstructed with p10.15.01. In the J/ψ and $b\bar{b}$ samples, 0.5 minimum bias events were added.

3 Details of the road construction

The road algorithm is part of DORECO. The versions used for the data reconstruction were affected by a number of problems.

- The tracker is longitudinally shifted by about 3 cm with respect to the calorimeter. A transverse shift of 5 mm at 53° has also been observed [2]. None of these shifts was taken into account in DORECO.
- In most of the dataset considered, only axial CFT information was available. As a consequence, standard global tracks were reconstructed with poor efficiency. To overcome this difficulty, the so-called “Gtr333” tracks¹ have been used in this study.
- The calorimeter SCA non linearities [3] were not corrected.
- Finally, there was an inconsistency between the track reconstruction program, which assumed a reverse magnetic field polarity, and the road method, which uses the real polarity.

For all these reasons, a dedicated ROOT macro was written. In this macro, the road algorithm operates with any kind of tracks. Only central roads (*i.e.*, such that $|\eta_{\text{det}}| < 1$) are constructed. The shifts between the tracker and the calorimeter are corrected, and the inconsistency between the magnetic fields is cured. The SCA non-linearities are corrected using a program written by R. Zitoun, available in the `em_util` package [4]. In the following studies, this ROOT macro has been used for the data with Gtr333 tracks, whereas the DORECO output based on standard “Gtr401” tracks has been used for the Monte Carlo samples. In both cases, a minimal number of ten hits along the tracks was required, and a $p_T > 2 \text{ GeV}/c$ cut was applied.

The electron identification criteria are based on the amounts E_i of energy collected in the various floors within the road. Throughout this study, the road constructed with a *dismerge* parameter [1] value of 0.25 is used. The electromagnetic fraction EMF is defined as $(E_1 + E_2 + E_3)/E_{\text{tot}}$, where E_{tot} is the total energy collected within the road. The E/p ratio is calculated as $(E_1 + E_2 + E_3)/p$, where p is the electron candidate track momentum.

4 Electron identification efficiency

Events containing two “loose” electrons were first selected as follows:

- $E_1 > 0, E_2 > 0, E_3 > 0,$
- $EMF > 0.6,$
- $0.4 < E/p < 1.3.$

¹Gtr333 tracks are initiated in the SMT and propagated to the CFT in the transverse plane, allowing for one missing CFT layer.

Out of the original data sample, 329k events were retained. The distribution of the two discriminating variables EMF and E/p is displayed in Fig. 1 for the J/ψ Monte Carlo sample. The efficiency of the loose electron identification shows very little dependence on the electron transverse momentum p_T , as can be seen in Fig. 2, and is $\sim 97\%$ for $p_T > 2 \text{ GeV}/c$.

In the rest of this section, only those tracks identified as loose electrons are further considered. Tight electron identification criteria are also defined, as shown in Fig. 1:

- $EMF > 0.85$,
- $0.6 < E/p < 1.05$.

The tight electron identification efficiency slightly improves with p_T , as can be seen in Fig. 2. It exceeds 85% for $p_T > 5 \text{ GeV}/c$.

With the goal of observing a J/ψ signal in the data, invariant masses are constructed in each event containing a tight electron for all combinations of this tight electron with other loose or tight electrons in the event. In order to reduce the background, advantage is taken of the rather symmetric configuration for the transverse momenta p_{T1} and p_{T2} of the two electrons from a J/ψ decay: it is required that $|p_{T1} - p_{T2}|/(p_{T1} + p_{T2})$ be smaller than 0.6, which keeps 94% of the signal in the J/ψ monte Carlo, as shown in Fig. 3. The result is shown in Fig. 4 for opposite and same sign track pairs. The peak in the low mass region is due to tracks belonging to the same jet, while the bump for masses above $4 \text{ GeV}/c^2$ is due to low p_T tracks belonging to opposite jets. There is no obvious excess of opposite sign pairs in the J/ψ mass region.

Assuming that the two tracks of a pair originate from a single object, its transverse momentum, hereafter called the J/ψ candidate p_T , can be calculated as the vector sum of p_{T1} and p_{T2} . The result is shown in Fig. 5 as a function of the track pair invariant mass. The effect of the track momentum and p_T asymmetry cuts is visible at low masses and low p_T .

In the opposite sign distribution, there is a hint of an accumulation for masses around $3 \text{ GeV}/c^2$ at high p_T , not visible for same sign combinations. This is confirmed in Fig. 6 where the J/ψ candidate p_T is plotted for masses between 2.9 and $3.1 \text{ GeV}/c^2$. A clear excess of opposite sign pairs is visible at high p_T . Unless otherwise explicitly specified, only J/ψ candidates with $p_T > 12.5 \text{ GeV}/c$ are considered in the following. The resulting mass distribution is shown in Fig. 7 (left) where the J/ψ peak is now clearly visible.

The J/ψ peak becomes more conspicuous once two tight electrons are required, as can be seen in Fig. 7 (right). This J/ψ signal will now be used to determine the efficiency to tag as tight a loosely identified electron. In principle, this efficiency can be inferred from the ratio of the histograms displayed in Figs. 7-right and 7-left. The result is shown in Fig. 8 for opposite and same sign pairs. There is a clear excess in the ratio at the position of the J/ψ peak for opposite sign pairs, but it also appears that the probability to tag as tight a second loose electron is higher in the opposite sign case even outside the J/ψ region. As a consequence, the same sign pairs cannot be used to evaluate the background under the J/ψ peak. This background has to be determined from the side bands, using opposite sign pairs only.

The sum of two exponentials and a Gaussian has been used to fit the background and the J/ψ peak, respectively, in the two cases of at least one and of two tight electrons. The fit results are shown in Fig. 9. When only one tight electron is required, the Gaussian is centered at $2.95 \text{ GeV}/c^2$, has a width of $190 \text{ MeV}/c^2$, and contains $n_1 = 96$ combinations. In the case of two tight electrons, the Gaussian is centered at $2.98 \text{ GeV}/c^2$, has a width of $170 \text{ MeV}/c^2$, and contains $n_2 = 60$ combinations. The efficiency to tag as tight a loose electron is calculated according to the formula $\varepsilon = 2n_2/(n_1 + n_2)$, with a result of 77%.

The J/ψ mass peak is however difficult to fit in the case of at least one tight electron. If the center and width of the Gaussian are fixed to the values fitted when requiring two tight electrons, the number of combinations in the peak becomes $n'_1 = 87$, which leads to an efficiency of 81%. Altogether, it can be concluded that the efficiency of the road method to tag as tight a loose electron is 80%, with a few percent uncertainty. This value is somewhat lower than the 85% found in the Monte Carlo. Taking the Monte Carlo value for the efficiency to tag as loose an electron, the overall efficiency to tag as tight an electron is $\sim 77\%$ in the data. The transverse momentum range of the electrons considered in this study extends down to $3 \text{ GeV}/c$, as can be seen in Fig. 10.

The number of low p_T J/ψ 's can be evaluated by lowering the p_T cut down to $4 \text{ GeV}/c$, requiring two tight electrons. The mass distribution thus obtained is shown in Fig. 11. The fitted Gaussian contains 85 combinations. About 25 J/ψ 's with $4 < p_T < 12.5 \text{ GeV}/c$ are therefore found with two tight electrons identified.

5 Misidentification probability

To measure the misidentification probability, a clean sample of pions with no electrons has to be isolated. This was done using A. Schwartzman's macro [5] to select events containing a $K_S^0 \rightarrow \pi^+\pi^-$ decay.² The SMT track pair invariant mass distribution obtained in the data is shown in Fig. 12-left. The subsample retained after selecting the mass window $0.45 < m_{\pi\pi} < 0.55 \text{ GeV}/c^2$ contains about 37k events. The SMT tracks were next matched to `Gtr333` tracks, the pair invariant masses were recalculated, and the same K_S^0 mass window was selected (Fig. 12-right).

The p_T distribution of tracks with $|\eta_{\text{det}}| < 1$ and associated with a K_S^0 selected as described above is shown in Fig. 13. A transverse momentum cut at $3 \text{ GeV}/c$ retains 200 pion tracks with an average p_T of $3.7 \text{ GeV}/c$, to which the road algorithm was applied. In the Monte Carlo sample, 297 tracks matched to pions from K_S^0 decay satisfy the same angular and momentum cuts.

The distributions of the electromagnetic fraction EMF and of the E/p ratio are displayed in Fig. 14 for the data and Monte Carlo. In the data, four out of the initial 200 tracks are tagged as tight electrons, which gives a misidentification probability of $2 \pm 1\%$. Out of the 297 tracks selected in the Monte Carlo sample, nine are retained by the tight electron selection criteria, which leads to a $3 \pm 1\%$ misidentification probability, a value well compatible with that obtained in the data.

²This macro utilizes the V0 reconstruction package which performs a constrained fit. The selection criteria were the following: two opposite sign SMT tracks; vertex $\chi^2 < 15$; collinearity $p_T \cdot l_{xy} > 0.999$; transverse decay length $> 0.35 \text{ cm}$; vertex radius $< 2.75 \text{ cm}$ (first SMT layer); track impact parameters $> 0.1 \text{ cm}$; track $p_T > 0.3 \text{ GeV}/c$.

6 b-tagging with electrons

In order to investigate the ability of the road method to tag b jets with electrons, a sample of b-enriched jets was selected and compared to a sample of generic QCD jets.

The runs between 151000 and 153500 have been skimmed by the top-group and R. Van Kooten [6] with the following criteria :

- at least one local muon with $p_T > 5 \text{ GeV}/c$, associated with a 0.5-cone good jet with $p_T > 10 \text{ GeV}/c$. The association criterion is $\Delta R(\mu, \text{jet}) < 0.7$.
- $p_t^{\text{rel}}(\mu, \text{jet}) > 1 \text{ GeV}/c$. The transverse momentum p_t^{rel} of the muon relative to the jet axis is defined in Ref. [7].

The sample thus obtained is enriched in b jets, with a purity of about two thirds [7]. The bad runs from the JetMet group [8] have been removed from the analysis.

For the sample of generic QCD jets, 4787 events were selected from Run 149327, a run good for both the calorimeter and the tracker. These events were required to have fired one of the following triggers, unbiased with respect to electrons: 3CJT7, JT_95TT, JT_65TT, JT_45TT, JT_25TT, 2JT_LO, mulptxatxx_CJT5, mulptxctxx_CJT5, mulptxatxx_2CJT3.

In the b-enriched sample, exactly one muon-tagged jet is required. The local muon p_T and p_t^{rel} are displayed in Fig.15. The jet opposite to the muon tagged one is defined as the one which maximizes $\Delta\varphi(\mu\text{-tagged jet}, \text{jet})$ (Fig. 16). This azimuthal difference is required to be greater than 2.4. These opposite jets are furthermore required to be central ($|\eta_{\text{det}}| < 0.8$). The p_T distribution of the jets thus selected is shown in Fig. 17, as well as that of the central good jets of the generic sample. A $p_T > 20 \text{ GeV}/c$ cut retains 2275 b-enriched jets. In the generic sample, 2304 jets are selected, with a somewhat harder p_T spectrum.

Tracks are next associated with a jet if $\Delta R(\text{track}, \text{jet}) < 0.7$. The p_T spectra of the associated tracks are very similar in the two samples (Fig. 18.) A p_T cut at $4 \text{ GeV}/c$ selects 1377 tracks in the b-enriched sample and 1826 in the generic sample. The multiplicity of selected tracks is thus higher in the generic sample than in the b-enriched one (0.8 *vs.* 0.6). The average p_T of the selected tracks is $\sim 8 \text{ GeV}/c$ in both samples.

The distributions of the E/p ratio *vs.* the electromagnetic fraction EMF shown in Fig. 19 do not suggest any obvious electron excess in the b-enriched sample. The tight electron identification criteria defined previously select 17 candidates in the b-enriched sample. In the generic sample, 16 presumably fake candidates are retained, corresponding to a misidentification rate of $\sim 1\%$. This rate is somewhat lower than that determined using K_S^0 decays, which may be due to the harder p_T range involved (an average of 8 *vs.* 4 $\text{ GeV}/c$).

Enrichment in electrons from b decay can be achieved by kinematic cuts. The transverse momentum p_t^{rel} of an electron track candidate with respect to the axis of the jet with which it is associated is defined as for muons, except of course that the electron momentum is not added to the jet. It can be seen in Fig. 20 that the shape of the p_t^{rel} spectrum is unaffected by the electron identification cuts in the generic sample, whereas the p_t^{rel} spectrum is shifted toward high values in the b-enriched sample, as expected for heavy flavours decays.

The same features are visible in Fig. 21 where the distributions of x_E vs. p_t^{rel} are shown for the b-enriched and generic samples, before and after identification cuts. The variable x_E is the fraction of the jet energy carried by the electron track. The cuts on these kinematic variables suggested in Ref. [1] are

$$(x_E > 0.35) \text{ .OR. } (p_t^{\text{rel}} > 0.75 \text{ GeV}/c).$$

They select 13 and 7 electron candidates in the b-enriched and generic samples, respectively.

An equivalent, maybe more convincing way, to show evidence of an electron signal in the b-enriched sample is to first apply the kinematic cuts and the electron identification criteria next. The kinematic cuts select 811 and 1029 tracks in the b-enriched and in the generic samples, respectively. A hint of electron signal may be visible in Fig. 22, where the distributions of the E/p ratio vs. the electromagnetic fraction EMF are shown for both samples.

This signal becomes more conspicuous if the EMF and E/p cuts are applied alternatively. In the b-enriched sample, the EMF distribution shows a clear excess for values close to unity once the $0.6 < E/p < 1.05$ cut has been applied. Similarly, there is an excess at the right location in the E/p distribution for $EMF > 0.85$. None of these excesses is seen in the generic sample.

If it is assumed that no real electrons are present among the 7 candidates selected in the generic sample, the expected background in the b-enriched sample amounts to 5 candidates, based on the number of tracks associated with a jet in both samples. It can thus be concluded that at least 8 real electrons are present among the 13 candidates selected in the b-enriched sample. This signal of (at least) eight electrons is to be compared to the expected number of electron-tagged b jets evaluated as detailed in Table 1:

Table 1: Estimate of the expected number of electron-tagged b jets.

Number of central jets with $p_T > 20 \text{ GeV}/c$ opposite to a muon-tagged jet		2275
b purity of the sample [7]	67%	1524
Back-to-back b jets [7]	33%	503
b \rightarrow e branching ratio	11%	55
$ \eta_{\text{det}}(e) < 1$ and $p_T(e) > 4 \text{ GeV}/c$ (b \bar{b} MC)	50%	28
Track reconstruction efficiency (b \bar{b} MC)	80%	22
Road efficiency (J/ψ data)	77%	17
Kinematic cut efficiency (b \bar{b} MC)	90%	15

In the initial muon-tagged sample, the b-purity is expected to be two thirds, and in one third of the cases the two b jets are emitted back to back [7]. The branching ratio for direct b \rightarrow e decays is 11%. Out of these electrons, 50% are central and have a p_T larger than 4 GeV/c. At this point, 28 b jets containing a “taggable” electron are expected to be present in the b-enriched sample. Taking from the Monte Carlo a probably over-optimistic track reconstruction efficiency of 80%, an efficiency of 77% for the road algorithm and the associated selection criteria, as determined from the J/ψ sample, and an efficiency of 90%

for the kinematic cuts, the expected number of electron-tagged b jets turns out to be 15. The difference between the expected and observed numbers of electron-tagged b jets in the b-enriched sample, *i.e.*, 15 *vs.* 8, may be due in part to an overly optimistic assumed tracking efficiency, and in part to an overestimated fake electron background level if real electrons are present among the candidates selected in the generic sample.

Finally, the efficiency to tag a b jet with an electron can be roughly compared with the tagging efficiency using muons.

- In the initial sample of events containing a muon-tagged jet, an additional back-to-back muon-tagged jet is found in nineteen events. Of those jets, 9 are central and have a p_T larger than 20 GeV/ c .
- In the same sample, there are 10 such jets (back-to back with a muon-tagged jet, central and with $p_T > 20$ GeV/ c) tagged by a tightly identified electron with $p_T > 4$ GeV/ c and $p_t^{\text{rel}} > 1$ GeV/ c .
- In the generic sample, there are 8 muon-tagged jets, to be compared to 4 jets tagged by a tightly identified electron with $p_T > 4$ GeV/ c and $p_t^{\text{rel}} > 1$ GeV/ c .

The performance of the electron tag is therefore at least as good as that of the muon tag³ (notwithstanding the fact that there is no soft electron trigger for the time being...). The probability to tag a b jet containing a “taggable” direct electron (the number of which was estimated to be 28 in Table 1) is about 35% using the $p_t^{\text{rel}} > 1$ GeV/ c cut, while the probability to tag a generic jet is 0.2%.

7 Summary and conclusion

Using a J/ψ signal, the efficiency of the road algorithm to tag an electron with the cuts

- $E_1 > 0, E_2 > 0, E_3 > 0,$
- $EMF > 0.85,$
- $0.6 < E/p < 1.05,$

has been determined to be 77%, with a few percent uncertainty, for central electrons with p_T above 3 GeV/ c . The probability to wrongly tag a pion with the same cuts and in the same p_T range is about 2%, as determined from a K_S^0 sample.

The possibility of b-jet tagging with electrons has been demonstrated, using the same electron identification cuts, for central electrons with $p_T > 4$ GeV/ c . To this end, kinematic cuts have to be used, such as $p_t^{\text{rel}} > 1$ GeV/ c or correlated cuts on p_t^{rel} and x_E . A b jet containing a direct decay electron, central and with $p_T > 4$ GeV/ c , can be tagged with an efficiency of about 35%, for a probability well below 1% to tag a generic jet.

³It has been verified that lowering the p_T cut from 5 to 4 GeV/ c does not change the performance of the muon tag

References

- [1] F. Beaudette and J.-F. Grivaz, *The Road Method (an algorithm for the identification of electrons in jets)*, D0 Note 3976.
- [2] F. Beaudette, EM-ID meeting, April 24, 2002:
http://www-d0.fnal.gov/phys_id/emid/d0_private/minutes/20020424florian.pdf
- [3] R. Zitoun, *Study of the non linearity of the D0 calorimeter readout chain*, D0 Note 3997.
- [4] Link to ROOT macros from the the EM-ID Certification Results web-page.
- [5] A. Schwartzman,
V0 reconstruction web-page :
http://www-d0.fnal.gov/~sch/d0_private/V0/V0.html
“K0 reconstruction”, D0 collaboration meeting, November 2001
http://www-d0.fnal.gov/~sch/d0_private/talks.html
- [6] b-ID group web-page:
Working with the Data: Taggers, Macros, Control Samples & Tools.
- [7] O. Peters, *Certification of b-jet tagging with a muon V1.0.*
- [8] JetMET-ID group web-page:
http://www-d0.fnal.gov/~d0upgrad/d0_private/software/jetid/certification/Macros/runsel.html

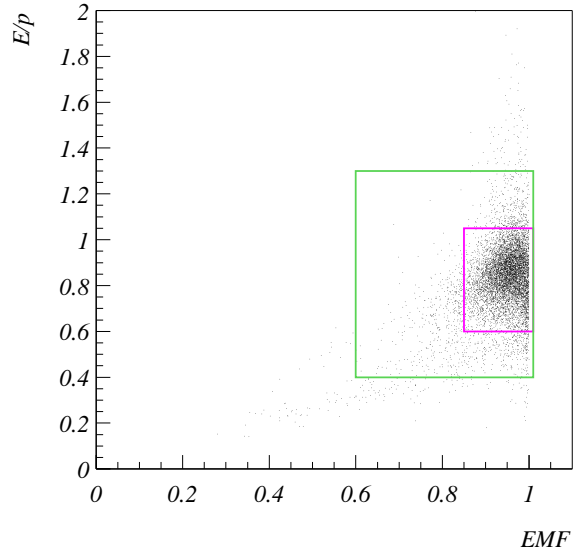


Figure 1: E/p vs. EMF in the J/ψ Monte Carlo sample. The loose and tight electron selection cuts are indicated.

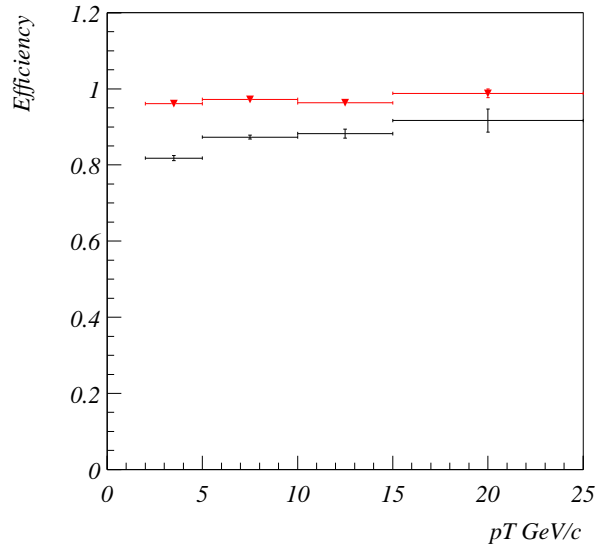


Figure 2: Loose (red triangles) and tight (black) electron identification efficiencies as a function of p_T in the J/ψ Monte Carlo sample.

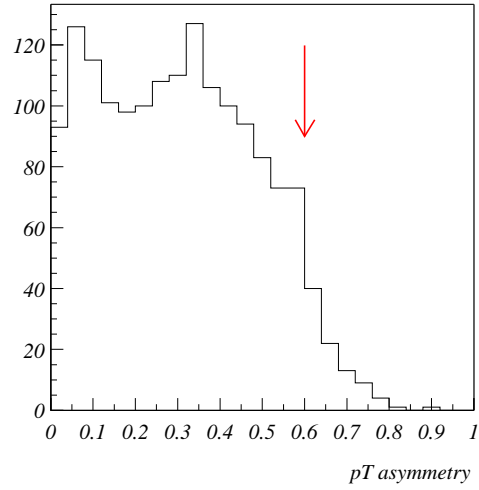


Figure 3: The p_T asymmetry between the two electron tracks in the J/ψ Monte Carlo sample.

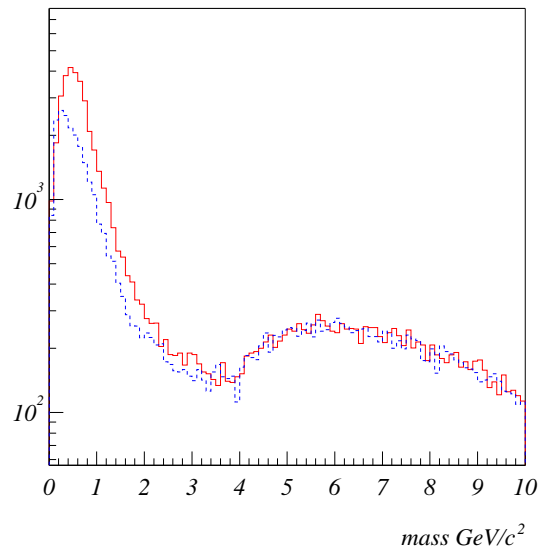


Figure 4: Invariant mass distribution of opposite sign (red) and same sign (dashed blue) pairs with at least one tight electron.

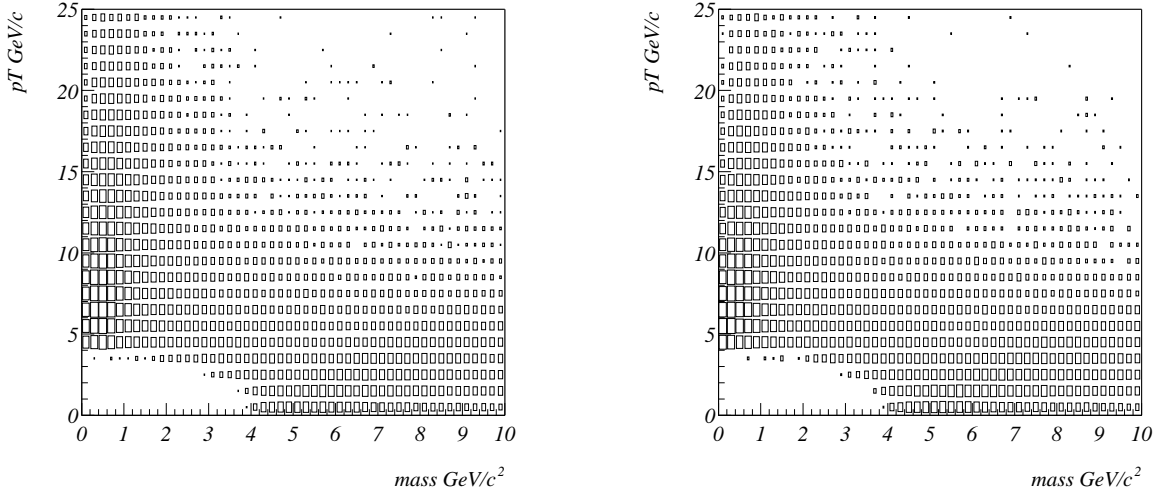


Figure 5: J/ψ candidate p_T vs. invariant mass for opposite sign (left) and same sign (right) pairs.

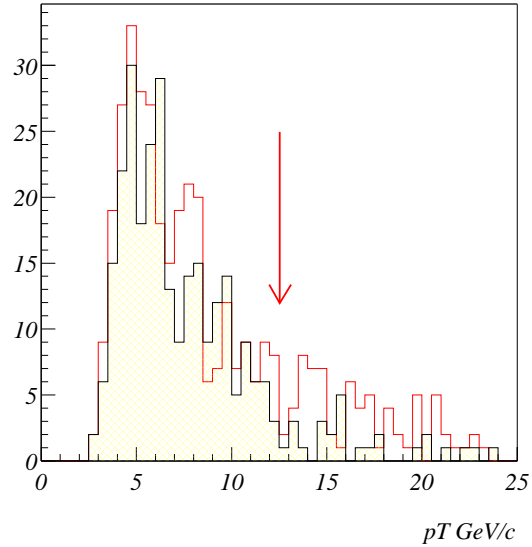


Figure 6: J/ψ candidate p_T for opposite sign (open histogram) and same sign (shaded histogram) pairs in the mass range from 2.9 to $3.1 \text{ GeV}/c^2$.

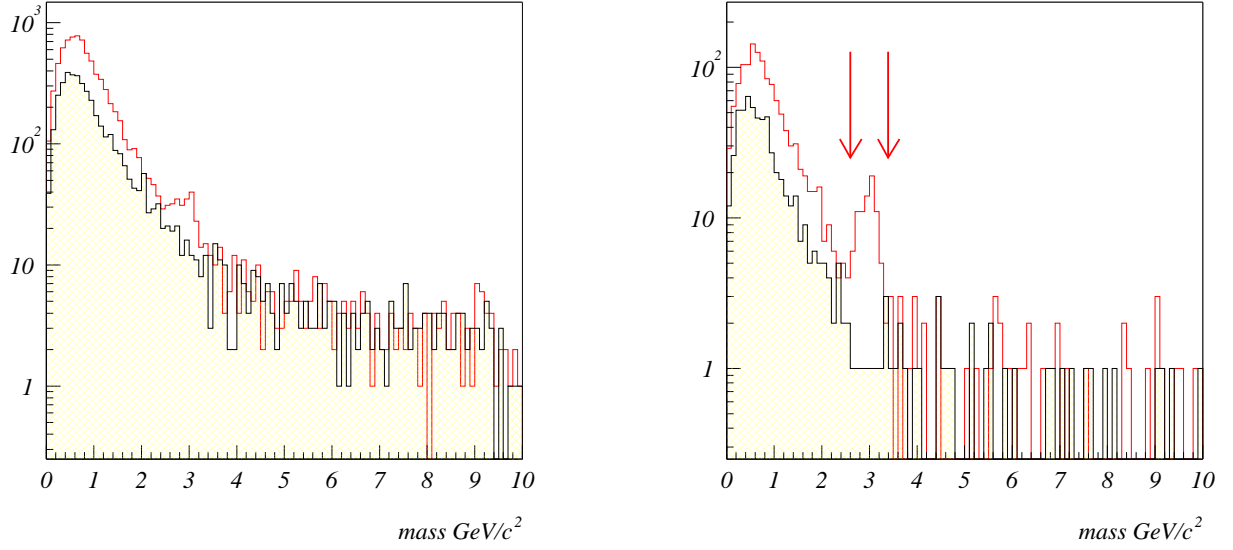


Figure 7: Invariant mass of opposite sign (open histogram) and same sign (shaded histogram) high p_T pairs, requiring one (left) or two (right) tight electrons.

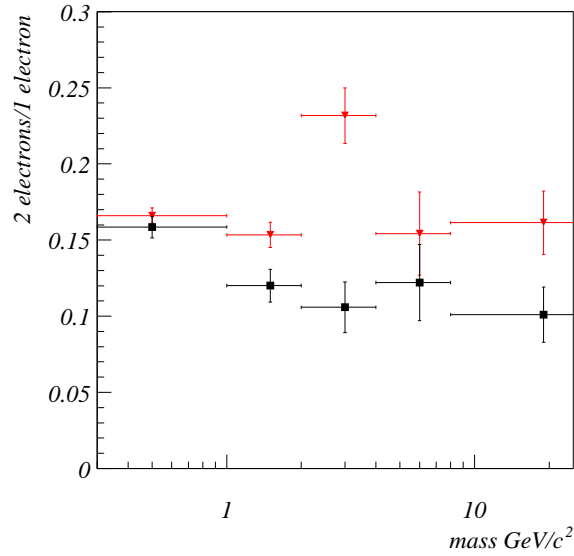


Figure 8: Probability to tag as tight a second loose electron, as a function of the pair mass for opposite sign (red triangles) and same sign (black squares) pairs. The horizontal scale is logarithmic.

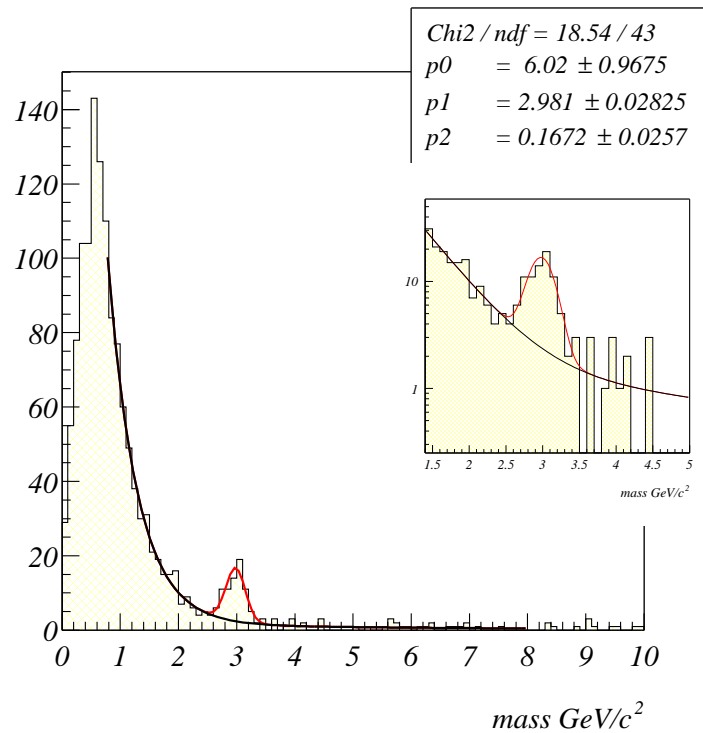
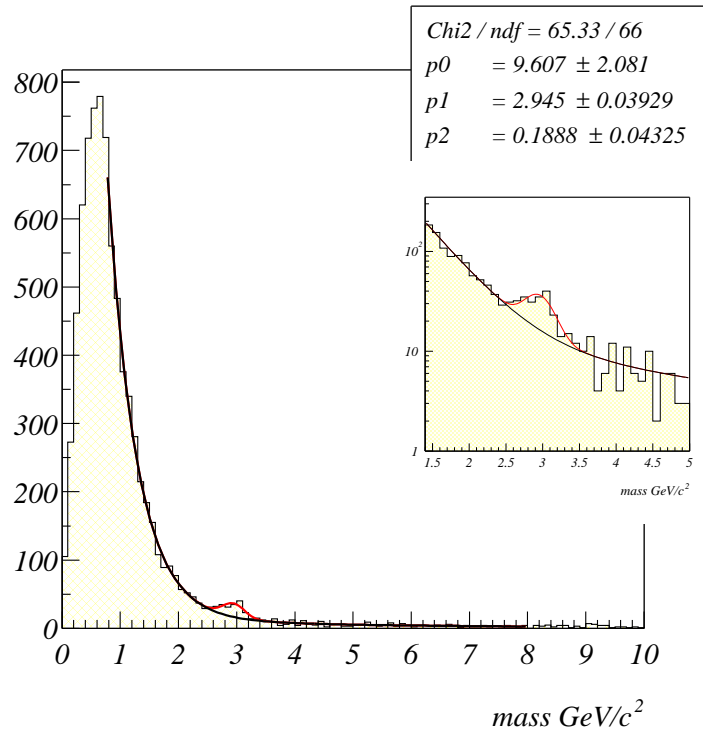


Figure 9: Invariant mass of opposite sign pairs for one (top) and two (bottom) tight electrons.

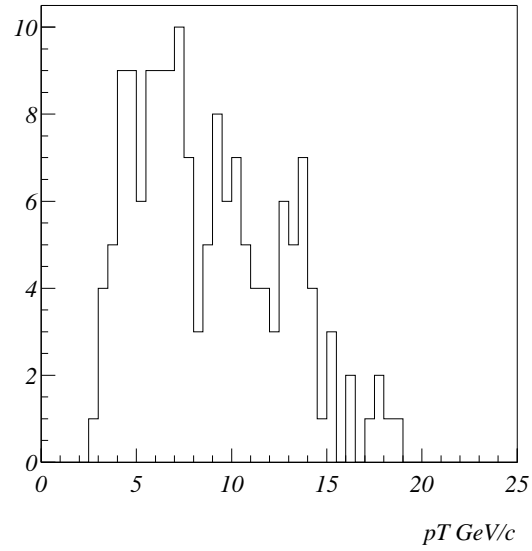


Figure 10: The p_T spectrum of tracks belonging to opposite sign pairs containing two tight electrons, in the mass range from 2.6 to 3.4 GeV/c^2 .

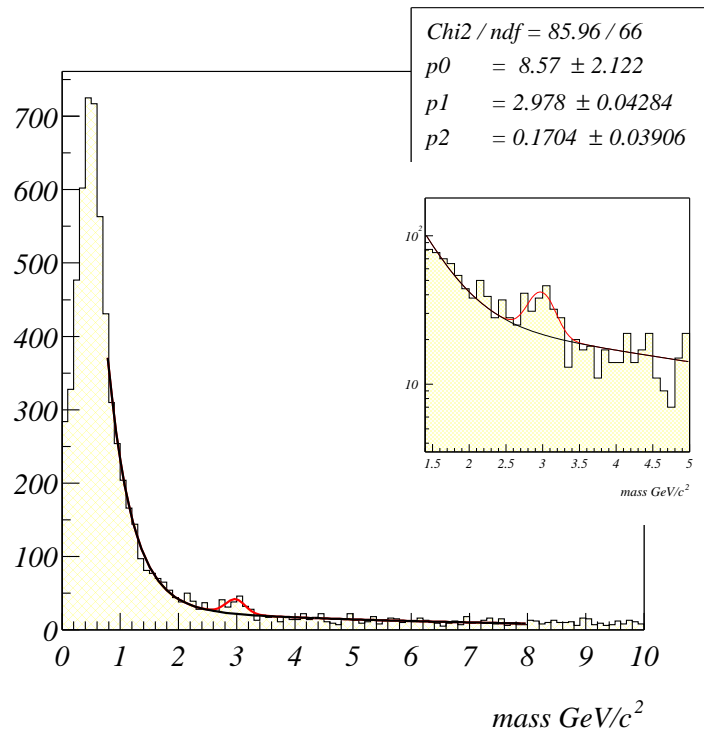


Figure 11: Invariant mass distribution for two tight electrons with a J/ψ p_T cut at 4 GeV/c .

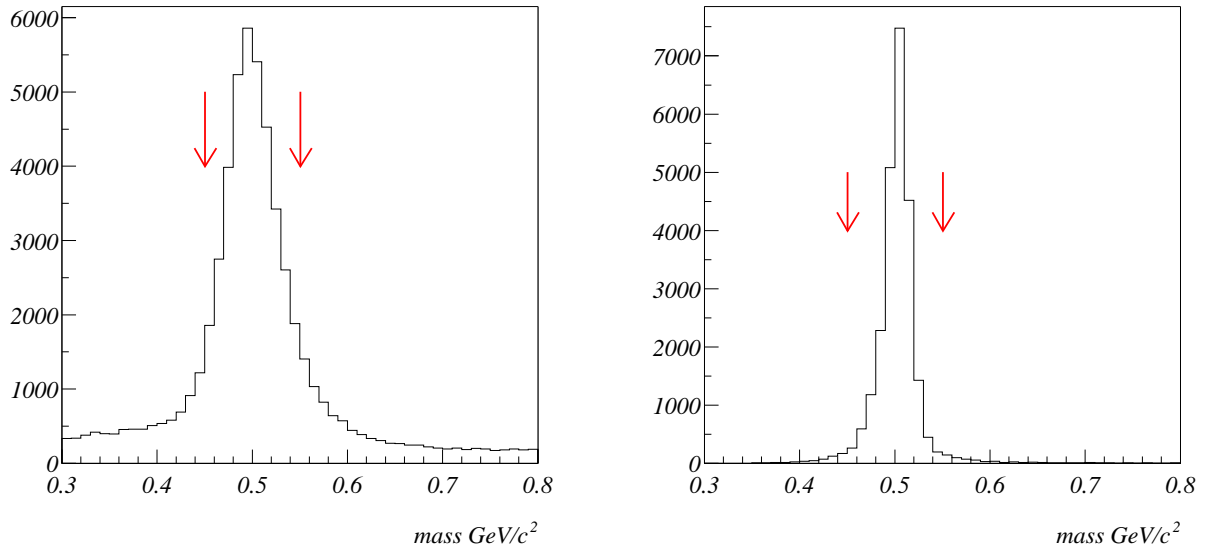


Figure 12: Track pair invariant mass using SMT tracks (left) and Gtr333 tracks (right).

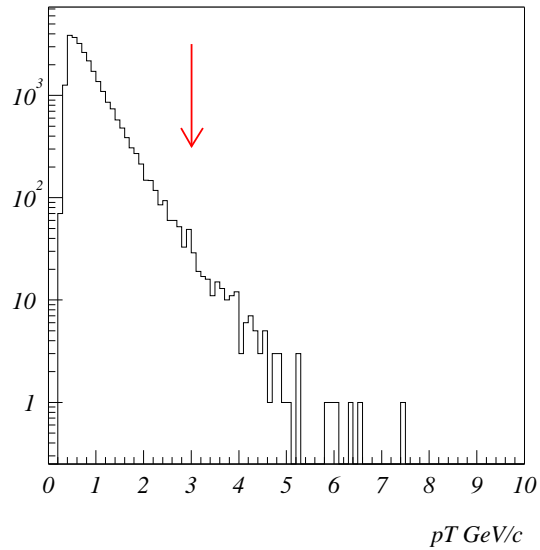


Figure 13: Transverse momentum of pion tracks in the K_S^0 sample.

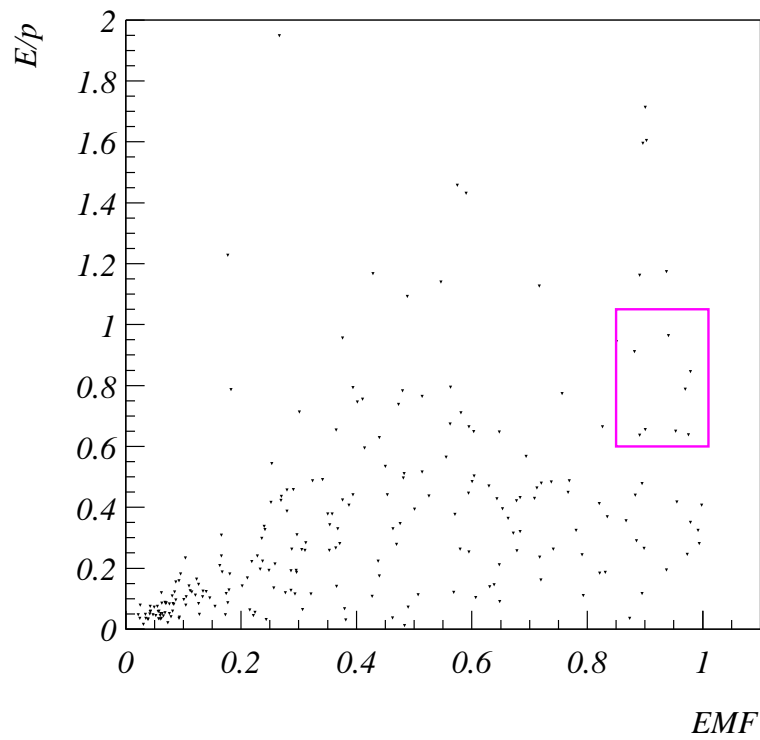
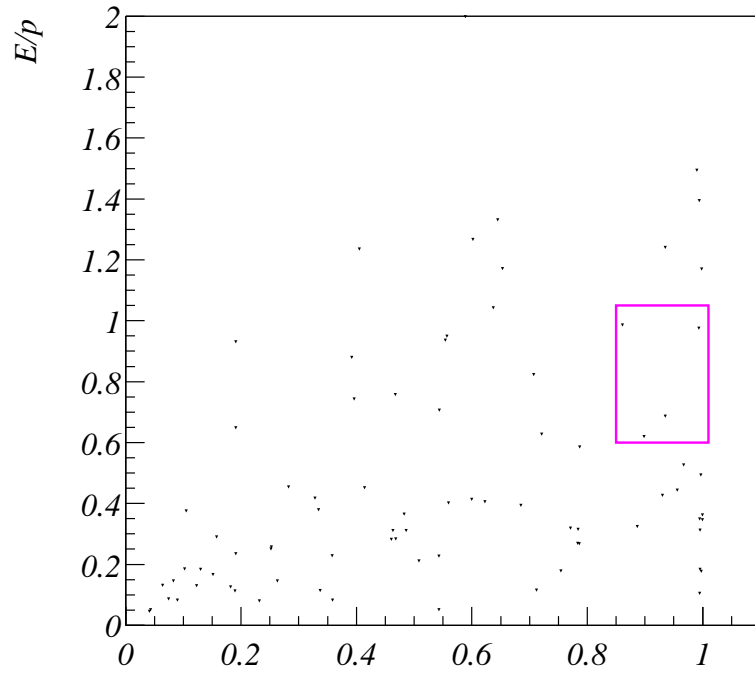


Figure 14: The E/p ratio *vs.* the electromagnetic fraction EMF in the data (top) and the Monte Carlo (bottom) K_S^0 samples.

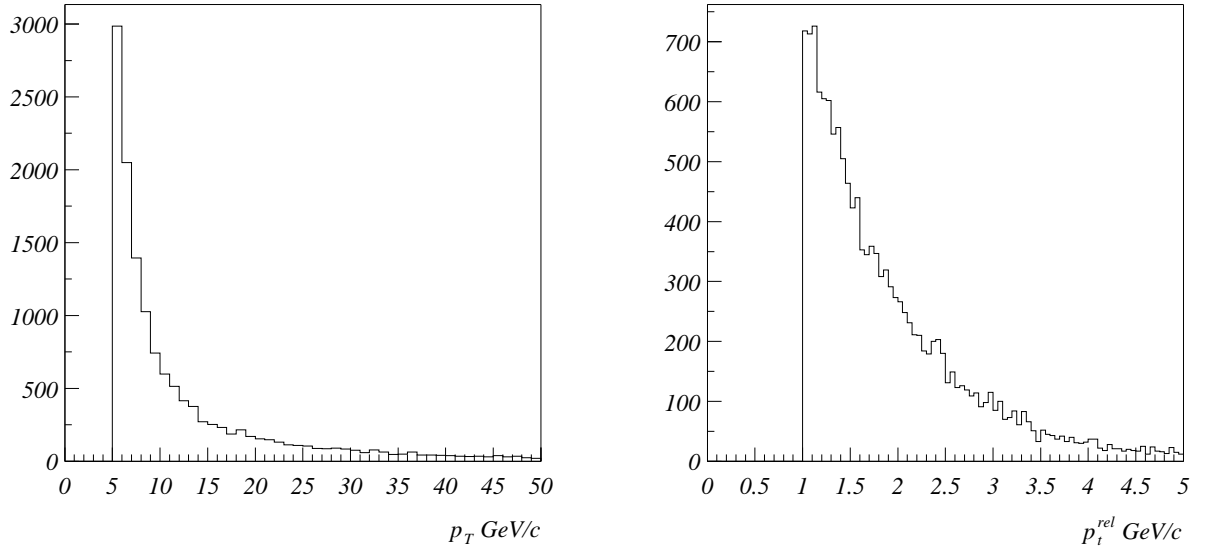


Figure 15: Local muon p_T (left) and p_t^{rel} (right) distributions in the b-enriched sample.

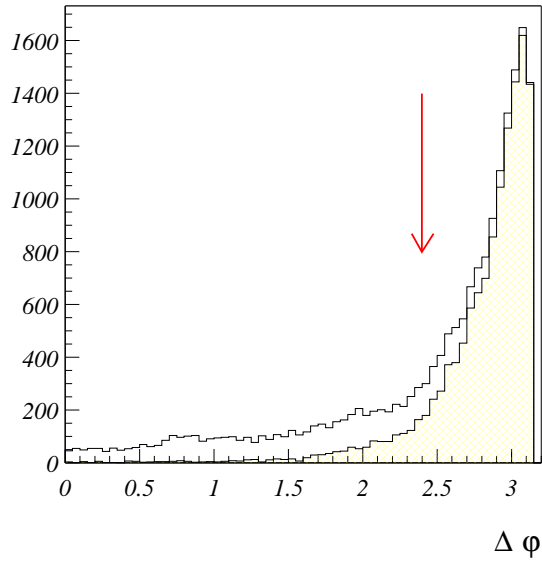


Figure 16: In the b-enriched sample, distributions of $\Delta\phi(\mu\text{-tagged jet, jet})$ for all jets (open histogram), and of its maximum (shaded histogram).

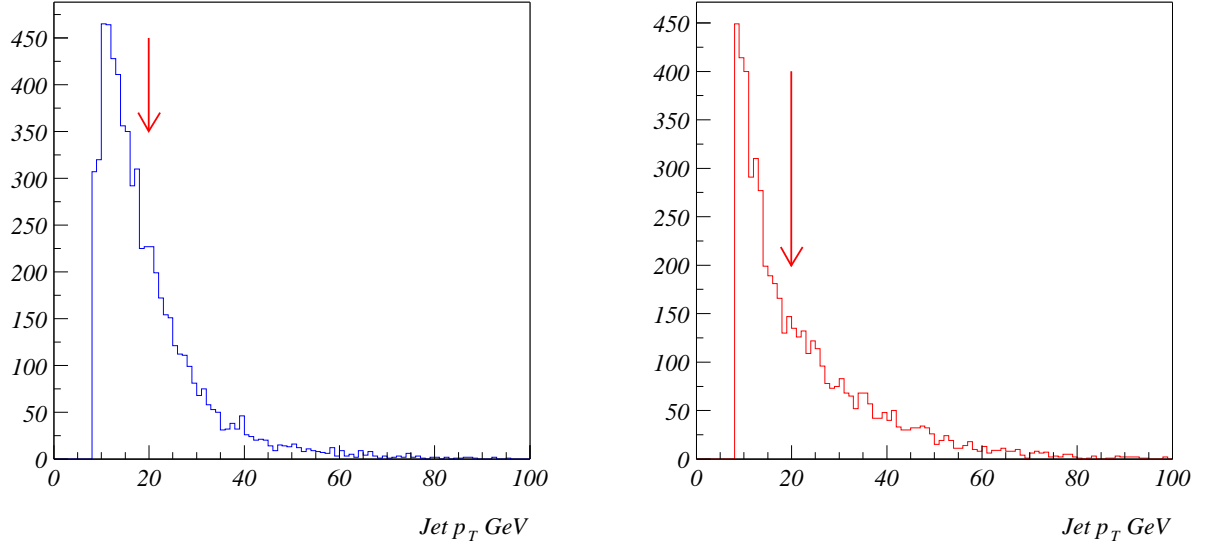


Figure 17: Jet p_T in the b-enriched sample (left) and for generic jets (right).

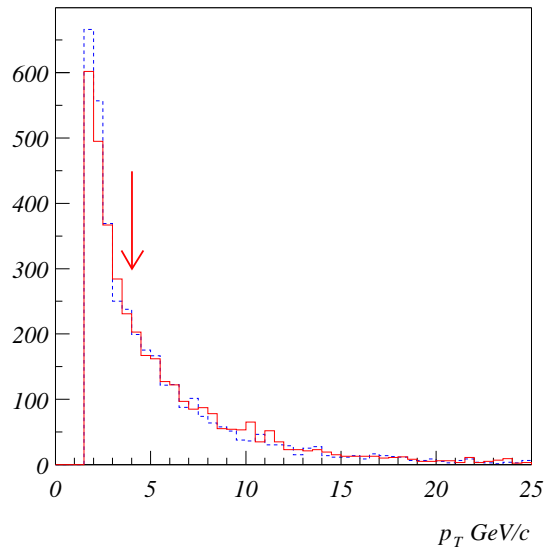


Figure 18: Transverse momentum distribution of associated tracks in the b-enriched (dashed blue) and in the generic (red) samples. The vertical scale is arbitrary.

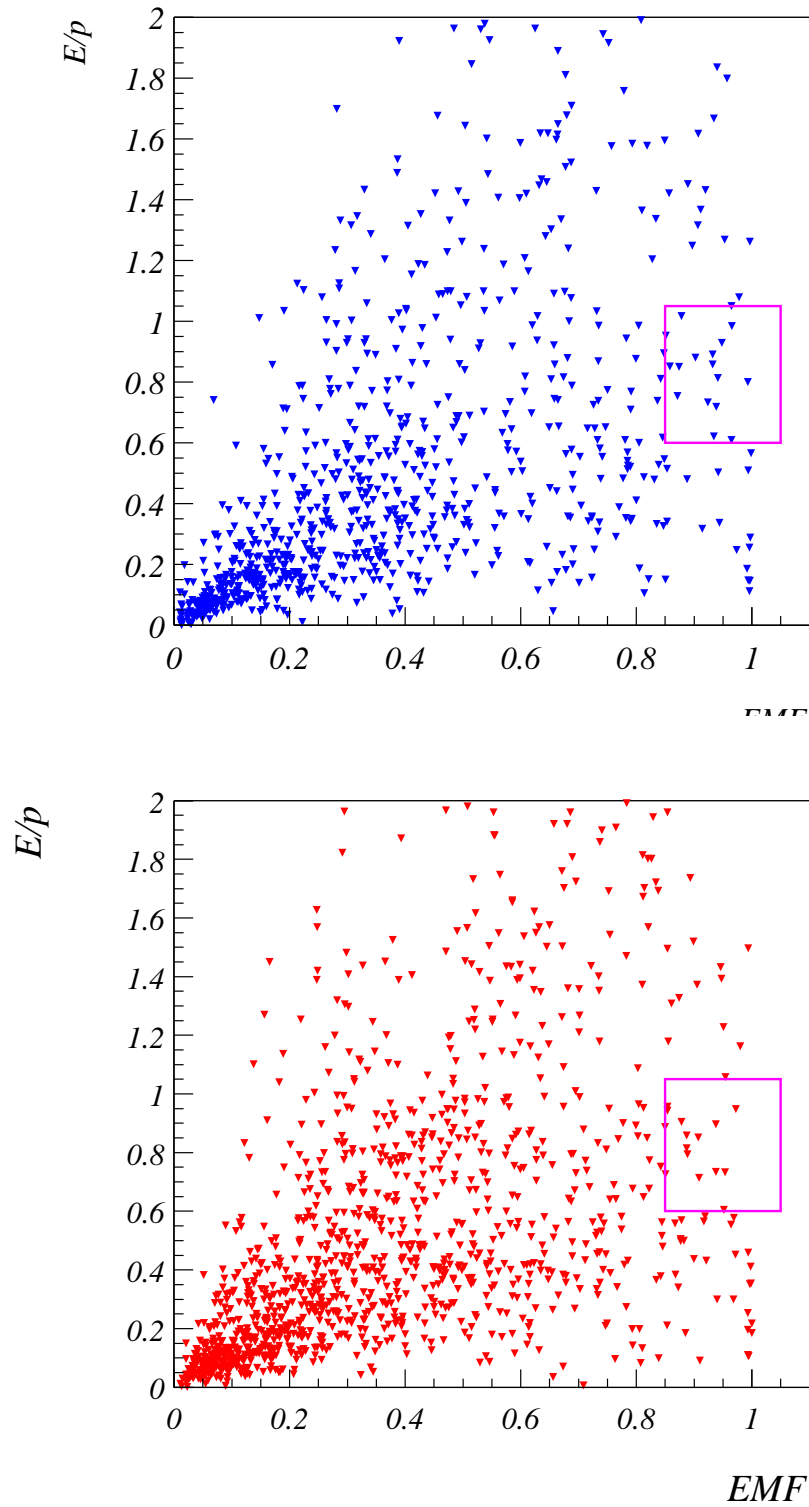


Figure 19: The E/p ratio *vs.* the electromagnetic fraction EMF in the b-enriched (top) and generic (bottom) samples.

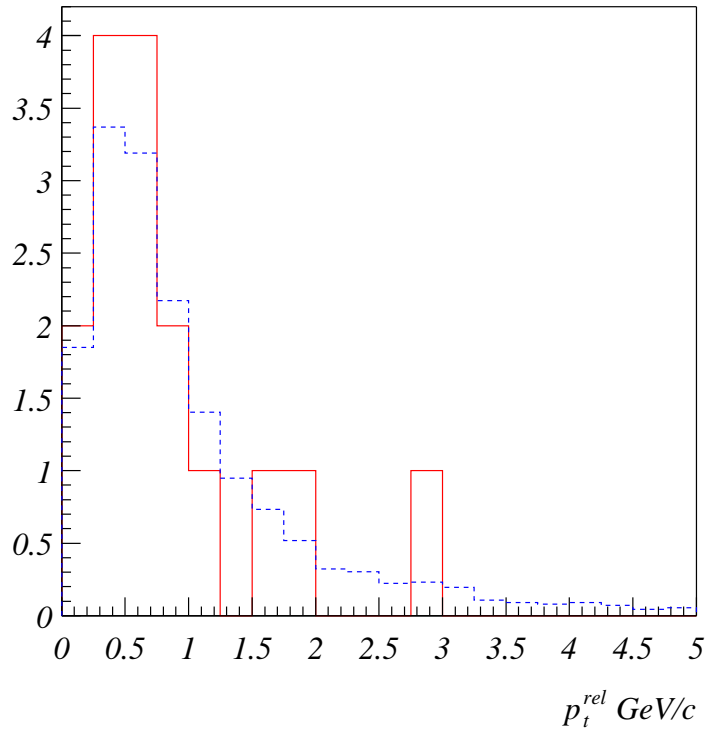
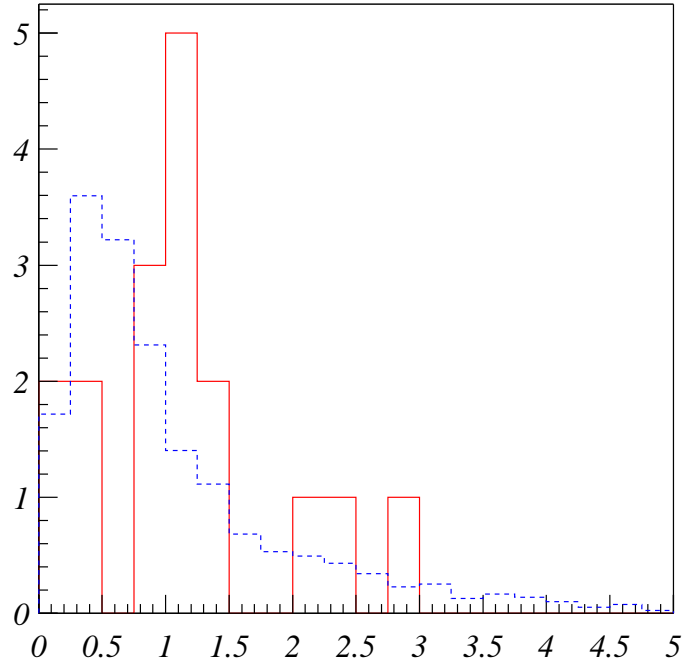


Figure 20: p_t^{rel} distributions before (dashed blue) and after (red) electron identification cuts in the b-enriched (top) and generic (bottom) samples. The distributions before identification cuts are normalized to those after cuts.

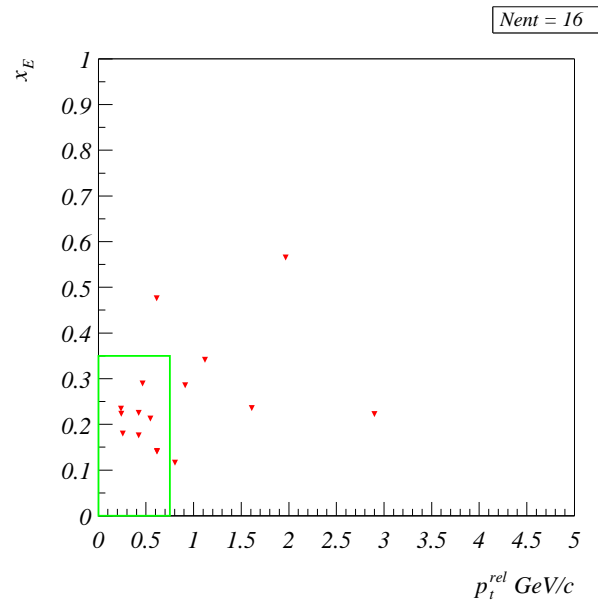
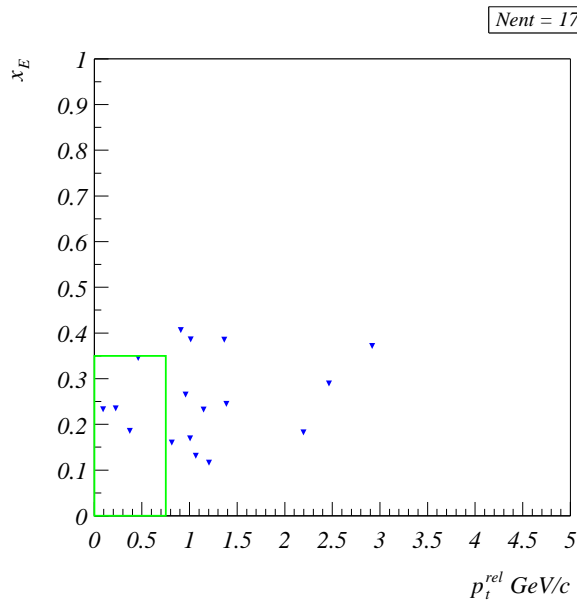
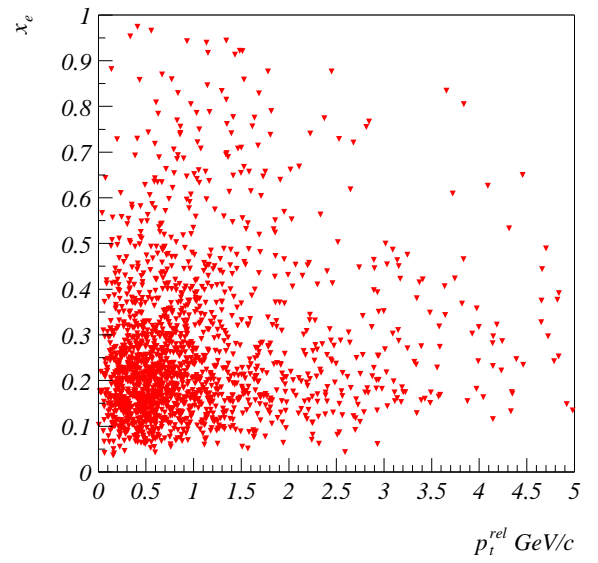
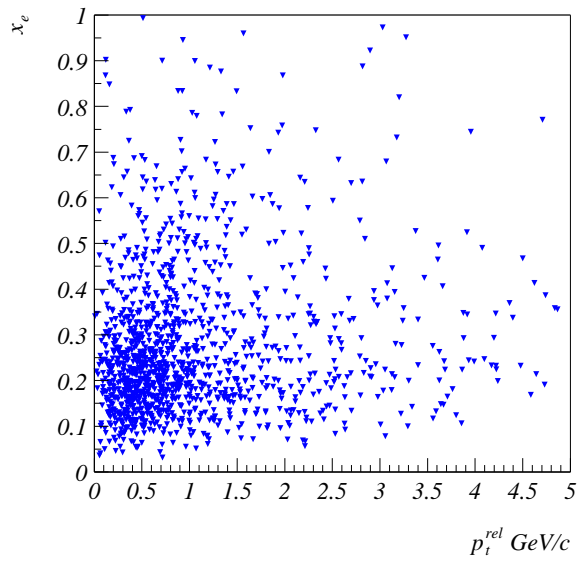


Figure 21: x_E vs. p_t^{rel} in the b-enriched (left) and generic (right) samples before (top) and after (bottom) electron identification cuts.

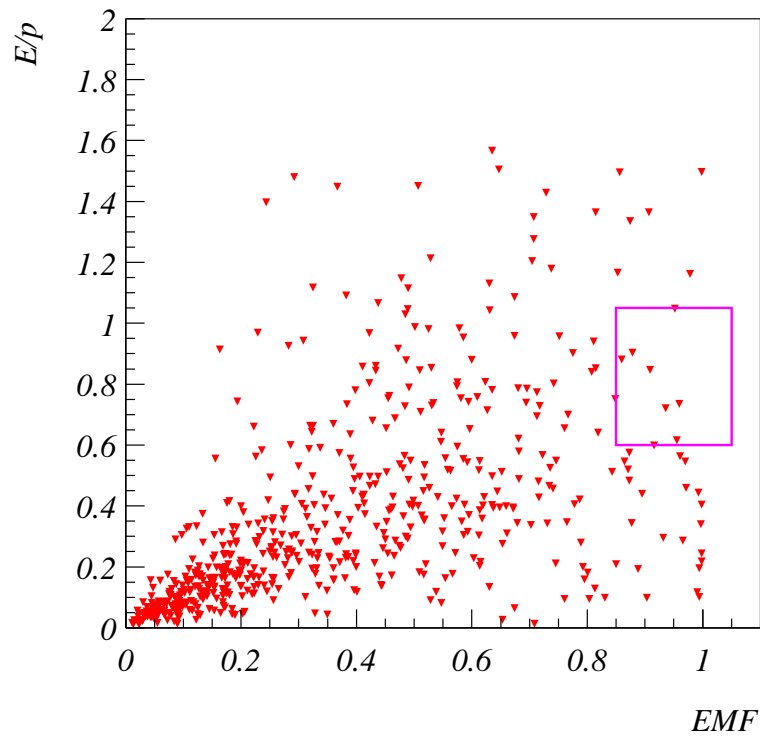
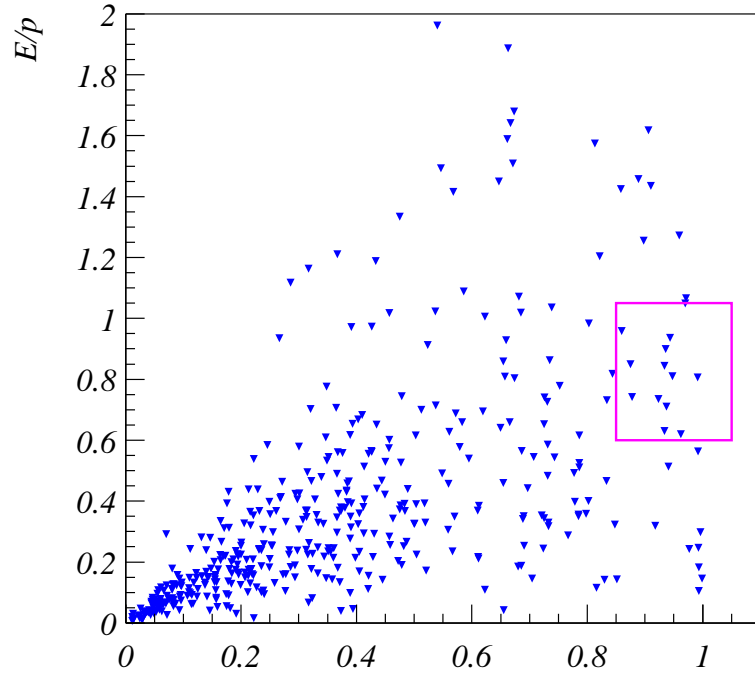


Figure 22: The E/p ratio *vs.* the electromagnetic fraction EMF in the b-enriched (top) and generic (bottom) samples after kinematic cuts.

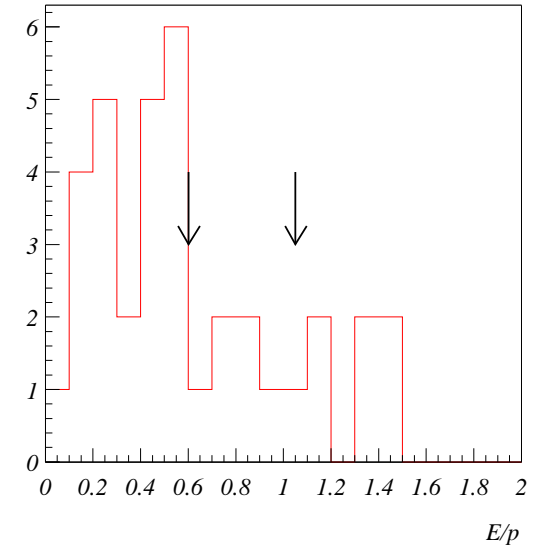
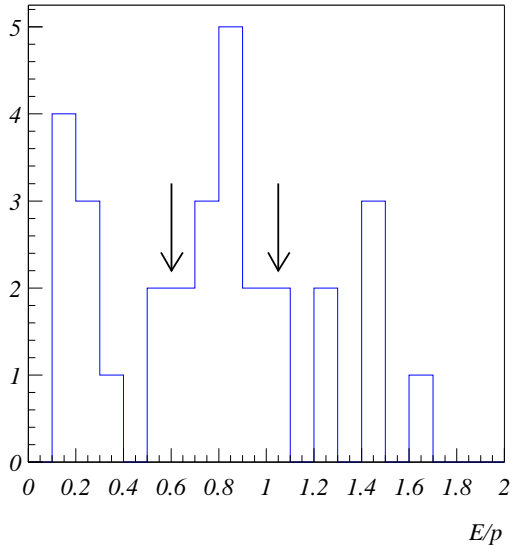
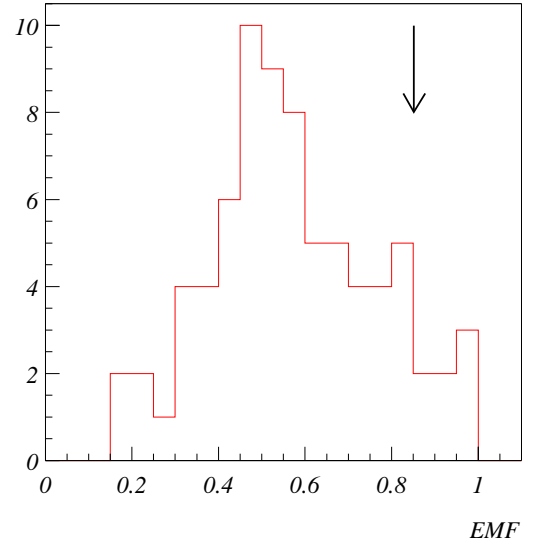
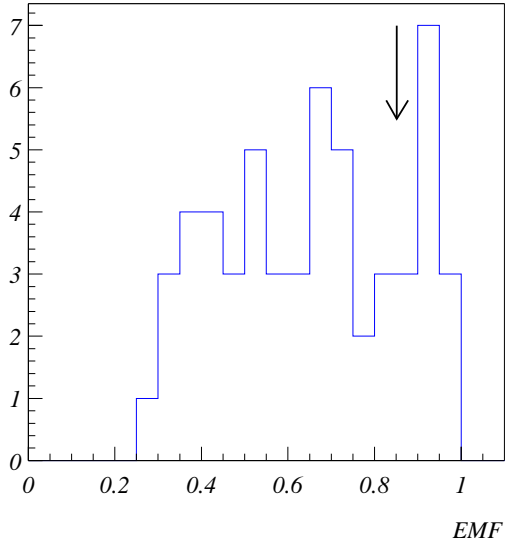


Figure 23: Distributions after kinematic cuts in the b-enriched (left) and generic (right) samples. Top: the electromagnetic fraction EMF for $0.6 < E/p < 1.05$. Bottom: the E/p ratio for $EMF > 0.85$.